

Magnetically Switchable Adhesion and Friction of Soft Magnetoactive Elastomers

Alexander Kovalev, Inna A. Belyaeva, Christian von Hofen, Stanislav Gorb,* and Mikhail Shamonin*

Herein, the effect of an applied moderate (≈ 240 mT) magnetic field on the work of adhesion (WoA) of mechanically soft (the shear modulus ≈ 10 kPa) magnetoactive elastomer (MAE) samples with two different mass fractions (70 and 80 wt%) of carbonyl iron powder (CIP) is concerned. The unfilled elastomer sample is used for comparison. Due to some sedimentation of filling particles, the concentration of inclusions in thin (≈ 10 μm) subsurface layers is different. It is shown that the WoA increases (up to 1.8-fold) on the particle-enriched side (PES) in the magnetic field and its value is higher for higher filler concentration. On the particle-depleted side (PDS), WoA does not depend on particle concentration and on the magnetic field. Adhesion and friction are coupled in MAEs. No statistically significant difference in the friction coefficient, determined from the extended Amontons' law, depending on sample side, CIP concentration, or presence of magnetic field is found. However, the PDS in the magnetic field demonstrates significantly higher critical shear stress compared to that for the PES or PDS in the absence of magnetic field. Correlations between different surface properties are discussed. Obtained results are useful for the development of magnetically controllable soft robots.

1. Introduction

Magnetically controllable adhesives currently attract growing interest, due to the possibility of switching between the adhesive and nonadhesive states by employing easily realizable magnetic fields generated by off-the-shelf permanent magnets or electromagnets.^[1] Current approaches include Gecko-inspired

adhesives where a magnetic field is used to actuate fibrillar structures,^[2–4] magnetorheological fluids (MRFs),^[5,6] magnetoactive (or magnetorheological) elastomers (MAEs),^[7,8] and embedding of MRFs into MAEs.^[1] Adhesive properties are crucial for soft robotics applications as far as gripping and retention are concerned. Furthermore, they are paramount for climbing locomotion, based on dry adhesion mechanism.^[9] It is also well known that adhesion and friction phenomena are often coupled.^[10,11] Hitherto, there is no complete understanding of the adhesion mechanisms of solid magnetic materials and their performance need to be optimized.^[1] In the past, artificial, switchable adhesive micro- and nanostructures have been fabricated, inspired by stimuli-responsive adhesive systems in nature. The stimulus, which enables the switching of surfaces from an adhesive to a nonadhesive state or vice versa can also have mechanical^[12–14]


or thermal^[15–17] nature. Bio-inspired light-controlled, reversible adhesive systems have been developed recently as well.^[18,19]

MAEs are hybrid materials,^[20] where micrometer-sized ferromagnetic particles (inorganic constituent) are embedded into a compliant elastomer matrix (organic constituent).^[21–29] We believe that MAEs are novel promising materials for applications in soft robotics, which are presumably capable of adhesion and friction control, because large changes in the work of adhesion (WoA) can be potentially achieved in moderate magnetic fields. It is obvious that adhesion depends on many structural and physical parameters of surface, in particular, surface roughness (SR) and that adhesion and friction properties are closely related and therefore should be studied simultaneously. MAEs become a very popular field of research in recent years because of exceptionally large changes of different physical properties (e.g., magnetorheological [MR] effect, magnetoresistive and magnetodielectric effects, magnetodeformation, etc.), which are of interest for a number of applications (e.g., vibration isolators and dampers, linear and rotary actuators for soft robotics, etc.).

Hitherto, the majority of works on MAEs concentrated on bulk properties of these materials. However, it has been recently understood that MAEs are promising materials for realization of stimuli-responsive (“smart”^[30]) surfaces, where the surface properties can be controlled by an external magnetic field. Specifically, it has been shown that the wettability,^[31–36]

A. Kovalev, C. von Hofen, S. Gorb
Department Functional Morphology and Biomechanics
Zoological Institute of the University of Kiel
Am Botanischen Garten 1–9, D-24118 Kiel, Germany
E-mail: sgorb@zoologie.uni-kiel.de

I. A. Belyaeva, M. Shamonin
East Bavarian Centre for Intelligent Materials (EBACIM)
Ostbayerische Technische Hochschule (OTH) Regensburg
Seybothstr. 2, D-93053 Regensburg, Germany
E-mail: mikhail.chamonine@oth-regensburg.de

 The ORCID identification number(s) for the author(s) of this article can be found under <https://doi.org/10.1002/adem.202200372>.

© 2022 The Authors. Advanced Engineering Materials published by Wiley-VCH GmbH. This is an open access article under the terms of the Creative Commons Attribution License, which permits use, distribution and reproduction in any medium, provided the original work is properly cited.

DOI: 10.1002/adem.202200372

the SR,^[37–42] as well as drop splashing^[43] depend on the applied magnetic field. The main physical reason for that is believed to be the magnetic-field-induced restructuring of the filler (changes in the mutual arrangement of magnetized inclusions) due to magnetic forces between the particles. It can be expected that this restructuring will be noticeable on the free surface of soft MAE materials and that the corresponding modifications of surface properties should be quite significant. In MAEs cured in the absence of magnetic field, the spatial distribution of ferromagnetic microparticles is isotropic in the absence of magnetic field, while in the presence of the field, the particles are rearranged into chain-type aggregates preferentially oriented along the magnetic flux lines.^[34] If the field is oriented perpendicular to the surface, this effect is expected to lead to the formation of conical surface structures (designated as “mountains” by Maman and Ponsinet^[44]) with the top of a “mountain” coinciding with the end of a particular chain-like aggregate. Such conical structures are well known from MR fluids. However, the elastomer network of MAEs imposes various configurational constraints that may result in a more complex topographical restructuring. Given that surface topography and subsurface (bulk) mechanical properties of soft MAEs change in an applied magnetic field, it is obvious that both adhesion and friction properties of MAEs should be field dependent as well.

Experimental studies of adhesion properties of flat samples from MAEs^[7,8] and their combinations with other materials^[1,45,46] have been reported in the literature. The adhesive force was typically determined by the lap shear testing. Also an alternative idea has been explored, where magnetic field has been used to control filamentary microstructures on the surface of an MAE material.^[3,4,32,47] Applications of structured MAE surfaces as suction^[47] and adhesion grippers^[48] have been also reported. The Young’s modulus of a composite material reported in ref.[4] was about 400 kPa, and the elastic moduli of materials reported in refs. [3,45,47] were in the MPa range. The polymer matrices reported in refs. [7,8,32] were based on the commercially available Sylgard 184 silicone, for which it is known that the Young’s modulus is between 1.3 and 3.0 MPa, depending on curing temperature.^[49] The works by Li et al. and Kim et al.^[46,48] did not provide details on the elastic properties of used MAEs but reported usage of commercial elastomer compositions, where the Young’s modulus is usually in the MPa range, as polymer matrixes. It can be concluded that the majority of previous works relied on relatively stiff polymer matrices resulting in stiff MAE compositions in comparison to MAEs used in our experiments, where the shear modulus in the absence of magnetic field is in the order of 10 kPa. Assuming that MAEs are incompressible neo–Hookean solids,^[50] the corresponding Young’s modulus of them is threefold higher.

Although it is obvious that the magnetic-field-dependent adhesive properties and corresponding bulk (e.g., shear modulus) and surface (e.g., SR) properties of MAEs should be interrelated, the relationships between them seem to be a hitherto neglected aspect of research. The purpose of this paper is to fill this gap in our knowledge. We report here on the measurements of the SR, the WoA, and the surface elastic modulus of four random heterogeneous soft MAE samples. Furthermore, the relationships between the measured material parameters are discussed. Because the magnetically induced adhesion of the fabricated

samples is large, it has to be expected that its contribution to the kinetic friction is significant.^[51] To the best of our knowledge, the importance of the contribution of adhesion to the friction properties for this type of material is shown here for the first time. The technological originality of our work and the key to obtaining large response to a magnetic field is in the usage of soft MAEs with the shear storage modulus of the order 10 kPa and the filling factor by particles of the order of 70–80 wt%.

2. Results

The fabrication of MAE samples involves pouring of them into a Petri dish. Therefore, each sample has two circular surfaces. The upper surface is polymerized in contact with the air, while the bottom one is polymerized in contact with the smooth surface of a Petri dish. The differences between these surfaces can be easily seen in the ambient light: the upper surface is shiny while the bottom one is rather matt. It has been recently noticed that there is a thin ($\approx 20 \mu\text{m}$) depletion layer under the top surface of MAEs with a reduced concentration of magnetic particles.^[37] We will denote the upper side of the MAEs *particle-depleted side* (PDS). The bottom surface is denoted as *particle-enriched side* (PES).

For unfilled (pure elastomer) control samples, notations PDS and PES are senseless. However, we will keep them for sake of convenience and comparability. Then, the PDS refers to the upper side of the sample during fabrication, whereas the PES refers to its bottom side.

Figure 1 presents the results of measurements of the SR using a white light interferometer. As expected, the root-mean-square (rms) roughness increases in an applied magnetic field on both sides. It is observed that the surface perturbation is larger for the PES. The responsivity of the magnetic-field-induced SR to an applied magnetic field is $\approx 6 \mu\text{m T}^{-1}$ for the PDS and $\approx 17 \mu\text{m T}^{-1}$ for the PES. These results qualitatively agree with previously reported measurements,^[34] where only information about the PDS of an MAE sample is available. The distinction between both PDS and PES is reported for the first time. As expected, the presence of a magnetic field has no effect on the measurements of unfilled samples.

The increase in the roughness due the presence of a magnetic field is stronger on the PES than on the PDS. One could conclude that MAE roughness in the presence of magnetic field is determined by the concentration of CIP in the vicinity of the surface.

Figure 2 presents the results of measurements of the effective elastic modulus for both sides of unfilled and filled elastomer samples. Without the magnetic field, there is no difference in elastic modulus between both PDS and PES of MAEs. However, in the presence of the magnetic field, the PDS shows higher elastic modulus compared to the PES. Interestingly, that in the polymer sample without CIP, the PDS is softer than the PES. In the presence of the magnetic field, MAEs demonstrate higher elasticity modulus, which is higher at higher CIP concentration. The highest stiffening of the surface in the presence of the magnetic field is observed in samples with 80% of CIP. This result is in agreement with the measurements of the bulk shear modulus and can be attributed to the restructuring of filler

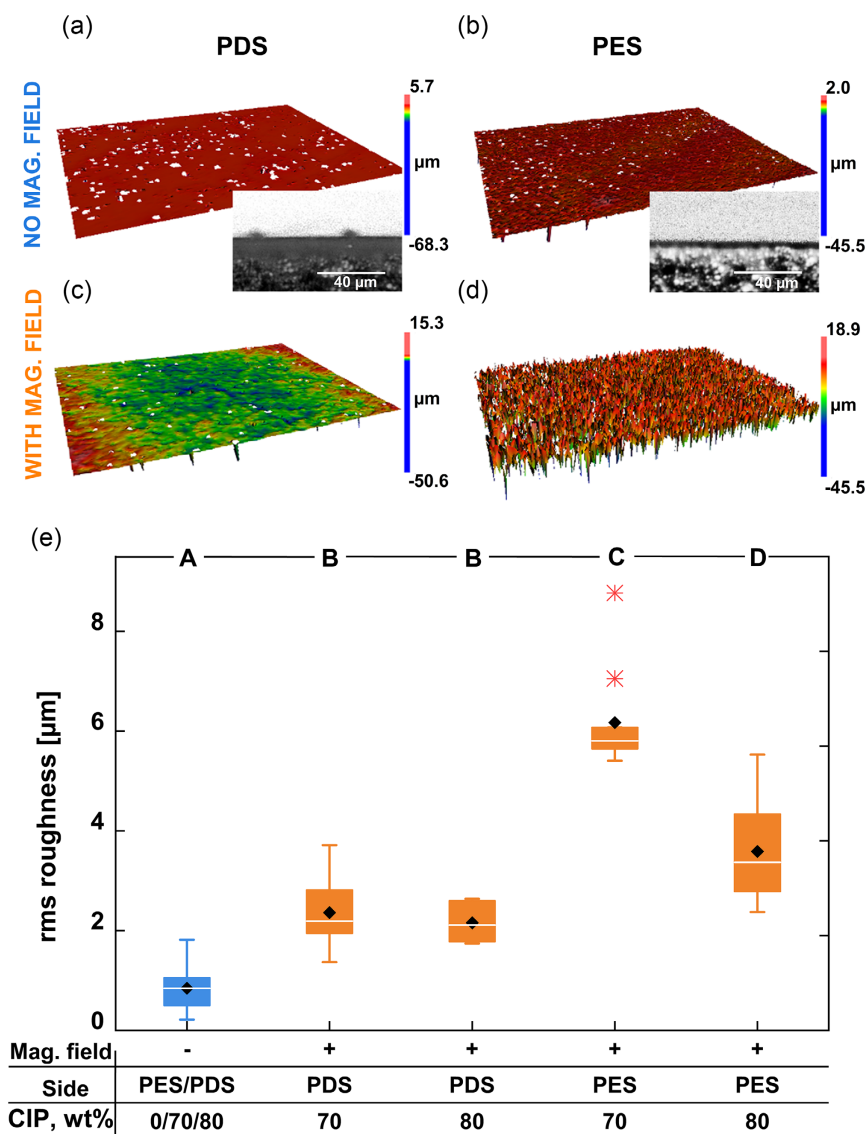


Figure 1. Roughness measurements on both sides of magnetoactive elastomer (MAE) samples. The subfigures (a) and (c) refer to the particle-depleted side (PDS) while the subfigures (b) and (d) refer to the particle-enriched side (PES). a,b) A typical surface profile in the absence of a magnetic field. c,d) A typical surface profile in the applied magnetic field. Size of the imaged area is 1.4 mm × 1.05 mm. The micrographs in the insets clearly demonstrate the differences between the PDS and PES. e) Roughness (root mean square, rms) on PDS and PES of MAE samples in the presence of magnetic field (indicated by “+”) at different carbonyl iron powder (CIP) concentrations. The blue color refers to measurements in the absence of magnetic field (indicated by “-”), the orange color refers to measurements in the maximum field. Black rhombus is the mean value, the white horizontal line is the median, edges of the box are 25th and 75th percentiles, whiskers are the extreme data values except outliers, which are marked with red asterisks. Different letters (A–D) in the upper row indicate statistically different groups of measurements. If the measurement results are denoted by the same letter, they are not significantly different. The first group A also includes the measurements on pure polydimethylsiloxane (PDMS) (without CIP) in the presence of magnetic field.

particles in the external magnetic field. The measured MR effect in MAE samples with 80 wt% of CIP is also larger than in samples with 70 wt% of CIP (Figure S2, Supporting Information). The MR effect, which is the relative ratio of the change in the shear storage modulus in the maximum magnetic field, $MRE = (G'(B = B_{max}) - G'(B = 0)) / G'(B = 0)$, was estimated to be about 14.3 for the samples with 80 wt% of CIP and roughly 8.0 with the samples with 70 wt% of CIP. In the earlier expression for MRE, B denotes the magnetic flux density and $B_{max} = 240$ mT.

The elastic modulus of both PDS and PES in the absence of magnetic field agrees with the order of magnitude of the effective shear modulus of all samples. The relation $E = 3G$, valid for incompressible neo-Hookean solids,^[50] must not be fulfilled because in our case the effective shear modulus refers to the low-frequency measurements in the bulk material while the effective elastic modulus refers to the static measurements of the surface region. It is also observed that the magnetic field affects the bulk shear modulus more strongly than the effective

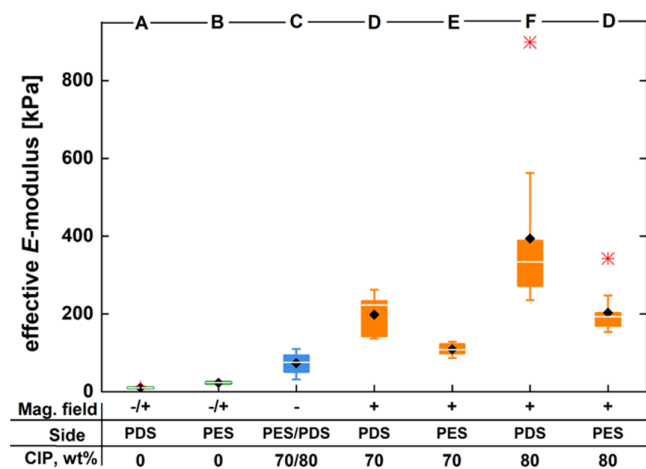


Figure 2. Influence of the magnetic field on the effective elastic modulus (E) of MAE samples with different CIP concentration measured on PDS and PES. Blue color refers to measurements in the absence of magnetic field (indicated by “-” in the table), orange color refers to measurements in the presence of the magnetic field (indicated by “+” in the table), green color refers to measurements performed both with and without magnetic field. White horizontal line is the median, black rhombus is the mean value, edges of the box are 25th and 75th percentiles, whiskers are the extreme data values except outliers, which are marked by red asterisks. Different letters (A–F) in the upper row indicate statistically different groups of measurements. If the measurement results are denoted by the same letter, they are not significantly different.

E -modulus, probably because the magnetic particles in the sample’s interior interact with more magnetic particles in the surrounding, while a magnetic particle in the vicinity of the sample’s surface effectively interacts only with particles in one half space.

Figure 3 depicts the WoA for both sides of unfilled and filled elastomer samples. The WoA on the PDS depends neither on CIP concentration nor on the presence of magnetic field. Therefore, the properties of a thin undersurface layer ($<150\ \mu\text{m}$, inset in Figure 1a) should determine the magnitude of the WoA. The WoA of MAE on the PES increases in the presence of a magnetic field and it is higher for the higher CIP concentration. This enhancement of the WoA on the PES correlates with the lower field-induced elastic modulus of the PES than that of the PDS (Figure 2) and with the magnetically enhanced roughness of the PES in comparison to that of the PDS (Figure 1). These effects may contribute to an increase in the WoA through the contact splitting mechanism.^[52]

To interpret the experimental data in friction experiments, we refer to the so-called extended Amontons’ law.^[10]

$$F_{\text{fr}} = \mu F_1 + \tau_0 A_{\text{real}} \quad (1)$$

where μ is the coefficient of sliding friction, F_{fr} is the tangential (friction) force, F_1 is the normal (loading) force, A_{real} is the real (true) contact area, and τ_0 is the critical shear stress. Equation (1) describes the friction force between dry surfaces that slide smoothly over each other in the presence of adhesion.^[10,53] Therefore, our model includes both adhesion-controlled and pressure-controlled friction phenomena. The details how the

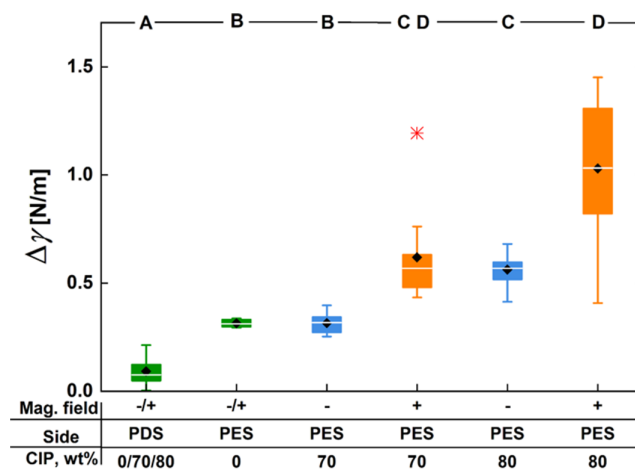


Figure 3. Effects of the magnetic field and CIP concentration on the WoA ($\Delta\gamma$) of MAE samples. Blue color refers to measurements in the absence of magnetic field (indicated by “-” in the table), orange color refers to measurements in the presence of the magnetic field (indicated by “+” in the table), green color refers to measurements performed both with and without magnetic field. White horizontal line is the median, black rhombus is the mean value, edges of the box are 25th and 75th percentiles, whiskers are the extreme data values except outliers, which are marked by red asterisks. Different letters (A–D) in the upper row indicate statistically different groups of measurements. If the measurement results are denoted by the same letter, they are not significantly different.

Equation (1) was fitted to the experimental data are given in Experimental Section.

In our experiments, we did not reveal any statistically significant difference in the friction coefficient (median value $\mu \approx 0.5$) depending on sample side, CIP concentration, or presence of the magnetic field, according to three-way analysis of variance (ANOVA). However, the PDS in the presence of magnetic field demonstrates significantly higher critical shear stress compared to that for PES or PDS without magnetic field (Figure 4). The friction force on the PDS in magnetic field has weaker dependence on loading. This means that the contact in magnetic field became more adhesive.

3. Discussion

Our measurements of the effective elastic modulus E , the WoA $\Delta\gamma$, the critical shear stress τ_0 , and the friction coefficient μ involve a sapphire ball, being in contact with a horizontal MAE surface, and moving either vertically (measurements of E and $\Delta\gamma$) or horizontally (measurements of τ_0 and μ). The measurement procedure and the data processing are described in detail in Experimental Section later. The sapphire ball with a diameter of 3 mm is nonmagnetic and rigid (elastic modulus $\approx 345\ \text{GPa}$).^[54] Its surface is very smooth ($R_a \approx 0.006\ \mu\text{m}$).^[55] An MAE surface is rather smooth (rms roughness $< 6\ \mu\text{m}$, cf. Figure 1), soft, and adhesive. To describe the force-displacement relationship for the contact between a rigid sphere with a diameter of 3 mm and a plane surface of a soft adhesive MAE material (tacky polymer), we used the well-known Johnson–Kendall–Roberts (JKR) model.^[56] Although this model

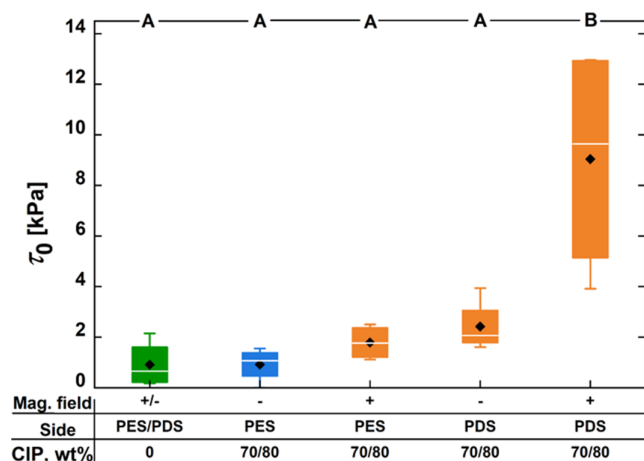


Figure 4. Effect of the magnetic field on the critical shear stress on PDS and PES sides of MAE samples. Blue color refers to measurements in the absence of a magnetic field (indicated by “-” in the table), orange color refers to measurements in the presence of a magnetic field (indicated by “+” in the table), green color refers to measurements performed both with and without a magnetic field. White horizontal line is the median, black rhombus is the mean value, edges of the box are 25th and 75th percentiles, whiskers are the extreme data values except outliers, which are marked by red asterisks. The letters (A–B) in the upper row indicate statistically different groups of measurements. If the measurement results are denoted by the same letter, they are not significantly different.

describes an idealized contact, it has been successfully applied in the past to fit experimental data and extract such material parameters as elastic modulus and surface energy.^[10,57]

Although the MAE materials in this study were very soft (shear modulus was in the order of 10 kPa), we did not observe any signs of material failure. The polymer network was strong enough to resist the mechanical friction or the magnetically induced surface deformation. The reason is that the maximal shear stress was sufficiently low, not more than 13 kPa.

It is well known that, in elastomers, the elastic modulus and the WoA counteract as reported by Fuller and Tabor.^[58] Such an effect was observed in our measurements as well: the elastic modulus of the PDS for both 70 wt% and 80 wt% CIP concentrations is higher than that of the PES in magnetic field, and the WoA of the PDS is lower than that of the PES. The larger change of the elastic modulus on the PDS can be explained by the protrusion of filling particles toward the MAE surface thus increasing the effective elastic modulus of the subsurface layer.

Surprisingly, both the elastic modulus and the WoA in the PES 70 wt% and the PES 80 wt% increase in the applied magnetic field. In this case, the increase in the WoA can be attributed to the significant increase in the surface roughness. It is known that microstructured surfaces may enhance adhesion.^[59]

The increased (4.7-fold) critical shear stress on the PDS of all MAE samples in the presence of magnetic field correlates (compared to other combinations of side and presence of magnetic field) with the approximately fourfold increase in the elasticity modulus on the PDS in the presence of magnetic field (calculated for samples with 80 wt% of CIP). Also, in the magnetically activated state, the PDS demonstrated higher elastic

modulus compared to the PES, it was 1.7 times higher for 80 wt% of CIP and 2.1 times higher for 70 wt% of CIP. Therefore, we can conclude, that the critical shear stress is observed because of the presence of adhesion, but it is independent of the exact WoA value. Instead, the critical stress is directly related to the elasticity modulus on the PDS in our experimental conditions.

Note that the observed magnetic-field-induced relative changes of the elastic indentation modulus E are severalfold lower than the relative changes of the (bulk) shear storage modulus. This means that the surface properties, in particular mechanical, are not trivially related to the bulk properties. However, the softness of the matrix is important for having significant particle rearrangements in an applied magnetic field causing the variations of surface properties.

4. Conclusion

Unexpectedly, our results demonstrate that the friction coefficient of investigated mechanically soft MAE does not depend on the applied magnetic field, if one correctly takes into account the effect of adhesion. The result shows that the contribution of adhesion is important in consideration of friction coefficient.

The adhesion significantly increases in the magnetic field (approximately, 1.8-fold) on the PES of MAEs, that is attributed to the significant increase in the surface roughness of the PES. In the magnetic field, the surface roughness increases less on the PDS than on the PES and the magnetically induced indentation modulus E is higher on the PDS than on the PES. Both effects seem to inhibit the change in the WoA on the PDS. To exploit such an increase in the WoA, MAE surfaces, similar to PES, should be tested in the future. From our previous preliminary work, we know that also upper MAE surface can be enriched with iron particles, if anisotropic MAE samples are synthesized. In anisotropic MAEs, the cross-linking is performed in a DC magnetic field (typically about 80 mT), perpendicular to the MAE surface. The particles arrange themselves into chain-like aggregates during cross-linking, and the ends of these aggregates come to the MAE exterior creating a rough surface. At the same time, the MR effect may be increased in anisotropic MAEs.^[29] Further research is required to investigate the friction properties of MAEs, in particular, how they can be affected by magnetic field. This paper demonstrates that the contribution of adhesion is important in consideration of friction coefficient. Investigation of adhesion and friction properties of anisotropic MAEs is an important problem, which should be addressed in the future work and might be potentially exploited in soft robotics.

5. Experimental Section

MAE Fabrication and Characterization: MAE samples were fabricated according to the already known protocol^[60,61] in several steps. First, a basic compound was made, consisting of polymer VS 100 000 (vinyl-functional polydimethylsiloxane), polymer MV 2000 (monovinyl functional polydimethylsiloxane), modifier 715 (SiH-terminated polydimethylsiloxane), all from Evonik Hanse GmbH (Geesthacht, Germany), carefully mixed with the silicone oil AK 10 (linear, nonreactive polydimethylsiloxane, Wacker Chemie AG, Burghausen, Germany). The next step was to make MAE

Table 1. Shear storage modulus in the absence of a magnetic field.

Sample	PDMS matrix	MAE 70 wt% of CIP	MAE 80 wt% of CIP
Shear storage modulus \pm standard deviation, Pa	2811 \pm 7	10 013 \pm 52	16 051 \pm 189

elastomers from the same basic compound, that is, with the same elastomer matrix. The only difference between the samples was the different concentration of soft-magnetic carbonyl iron powder (CIP) (type SQ, mean particle size of 3.9–5.0 μm , BASF SE Carbonyl Iron Powder & Metal Systems, Ludwigshafen, Germany).

The initial compound was mixed with CIP 70 wt% (≈ 22 vol%) and 80 wt% (≈ 33 vol%). A small volume of cross-linker CL 210 (dimethyl siloxane–methyl hydrogen siloxane copolymer comprising SiH groups) was then added, providing a soft elastomeric matrix (shear storage modulus $G' \approx 2.8$ kPa). In this case, the ratio r of the molar concentrations of vinyl and hydride groups in the initial compound with the addition of a cross-linker corresponded to $r \approx 0.61$.^[62] After careful mixing, Pt-catalyst 510 (0.33 wt% for the elastomer) was added to start the hydrosilylation reaction, the activity of which was controlled by the addition of divinyltetramethyldisiloxane inhibitor also supplied by Evonik Hanse GmbH (0.17 wt% for the elastomer).

The finished MAE mixture was thoroughly blended using a vacuum mixer to remove all air bubbles, and then poured into Petri dishes (diameter of 33 mm, Greiner Bio-One GmbH, Germany) to achieve a layer

thickness of about 1 mm. The filled Petri dish was placed in a vacuum desiccator for ≈ 5 min. Finally, MAE samples were cured in a universal oven (Memmert UF30, Memmert GmbH, Schwabach, Germany) with air circulation, first at 80 °C for 1 h and then at 60 °C for 24 h.

The MR characterization was performed using a commercially available rheometer (Anton Paar, model Physica Modular Compact Rheometer (MCR) 301), with a measuring “plate–plate” unit and a magnetic cell Magneto-Rheological Device (MRD) 170/1 T. Two fully cured samples in the form of a disk with a diameter of 20 mm, corresponding to two concentrations of iron particles, were cut out of the molds. The MR measurements were performed on these two specimens. Two other samples had a diameter of ≈ 30 mm, determined by the size of the Petri dish. The circular oscillation frequency ω was kept constant at 10 s^{-1} . A normal force of ≈ 1 N was applied to avoid slippage. The measurements were made at constant strain amplitude $\gamma = 0.01\%$, which corresponded to the linear viscoelastic regime. The results are shown in Figure S1, Supporting Information. The shear modulus of the matrix and the MAE samples are summarized in **Table 1**.

Characterization of an Applied Magnetic Field: Two cylindrical neodymium iron boron magnets (grade N42, dimensions $\varnothing 25 \times 5$ mm) were stacked together, with a protective silicone spacer between them. The magnetic field was measured in air along the symmetry axis of the stack using a gaussmeter with a Hall sensor. The distance between the top surface of the magnet stack and the bottom surface of an MAE sample was 2.7 mm. At this position, the magnetic flux density was ≈ 255 mT. At a distance of 3.7 mm (where the top surface of a sample would be positioned), the magnetic flux density was ≈ 231 mT. For estimations of the MR effect, the average magnetic flux density B_{max} of

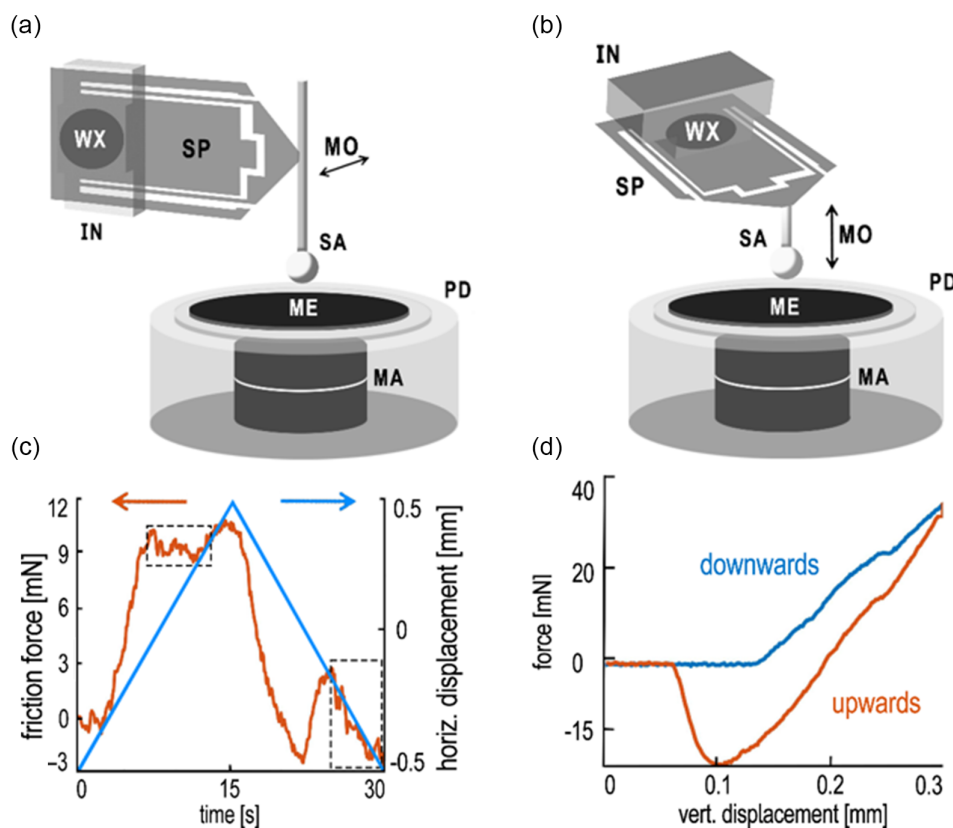


Figure 5. Measurements of a) the friction force and b) the pull-off force. c) Typical time dependences of the friction force (red curve) and the horizontal displacement (blue curve) of the sapphire ball (SA). Rectangular boxes surrounded by dashed lines indicate stick-and-slip episodes in the behavior of the sample. d) Typical dependences of the measured force on the vertical displacement of the SA. The blue curve corresponds to the downward movement of the SA, the red curve corresponds to the upward movement of the SA. Abbreviations: IN = instrument, MA = permanent magnet, ME = magnetic elastomer, MO = movement direction, PD = Petri dish, SP = double leaf spring, WX = wax.

240 mT was taken. If a point is positioned at the symmetry axis of the magnet, the magnetic field is directed perpendicular to it and, therefore, perpendicular to the MAE surface. All measurements were performed in the vicinity of the symmetry axis of the magnet, where the magnetic field can be considered homogeneous. The calibration curve for the magnetic field on the axis of magnets is given in Figure S2, Supporting Information.

Roughness Measurements: The rms roughness of MAE samples (Figure 2) was determined using the white light interferometer NewView 6000 (Zygo Middlefield, CT, USA) with 5× objective lens (N.A. 0.4, observation area size 1.4 mm × 1.05 mm), according to the protocol described by Salerno et al.^[63] Five measurements on five different locations were performed for each sample side.

Estimation of the E-Modulus and the Work of Adhesion Using JKR Micro-Indentation: Adhesion and friction measurements (Figure 5) were performed with microforce tester Basalt-1 (TETRA GmbH, Ilmenau, Germany)^[64] under laboratory-ambient conditions (temperature of 22–24 °C and relative humidity of 28–32%). MAE samples were indented by a sapphire ball (3 mm diameter) attached through a piece of the thick glass capillary to the end of a planar cantilever spring (spring constant of 320 N m⁻¹, Figure 5b). The approach and retraction speeds were 15.5 μm s⁻¹. The recorded force–displacement curves were used to calculate the elastic modulus (*E*) and the WoA ($\Delta\gamma$) at the tested location. For this purpose, an unloading part of the force–displacement curve $F_n(\delta)$ was fitted using an original MATLAB (Mathworks, Natick, MA, USA) program according to the JKR model

$$\delta = \frac{3\pi\Delta\gamma}{4E} \sqrt{\frac{R}{6}}^{2/3} \left(3\sqrt{1 - \frac{F_n}{F_p}} - 1 \right) \left(\frac{1}{2} + \frac{1}{2}\sqrt{1 - \frac{F_n}{F_p}} \right)^{1/3} \quad (2)$$

where δ is the vertical displacement of the ball with respect to the initial position of the MAE surface, F_n is the normal force, $F_p = -1.5\pi R\Delta\gamma$, R is the radius of the contacting ball.^[56,65] $\Delta\gamma = \gamma_1 + \gamma_2 - \gamma_{12}$, where γ_1 and γ_2 are the adhesive energies of the two surfaces and γ_{12} is the interaction term. Each of sample sides was tested at five different locations.

Since there might be ferromagnetic parts present in the commercial measurement devices used, we also performed all the measurements on unfilled (pure elastomer) control samples in the absence of magnetic field and in the maximum field. By doing so, we were able to estimate the influence of the magnetic field on the accuracy of measurements and to evaluate the significance of observed changes in MAE samples under maximum magnetic field.

Friction Measurements: Friction measurements were performed using the Basalt I device as well. For this purpose, the sapphire sphere was pre-loaded normal to the sample surface with 1–50 mN and moved parallel to the surface back and forth (the spring motion speed and distance were 77.9 μm s⁻¹ and 1 mm correspondingly, Figure 5a). Five cycles of backward and forward movements were performed on five different locations for each sample side. The effective friction (F_{fr}^*) and loading (F_l^*) forces were determined at five different loadings along second to fourth motion cycles (back and forth motion) in friction experiments according to the following expressions.

$$F_{fr}^* = \frac{1}{L} \oint F_{fr} ds, \quad F_l^* = \frac{1}{L} \oint F_l |ds| \quad (3)$$

where L is the total movement length of the sphere. The values of effective forces were used for estimation of the effective friction coefficient μ and the critical shear stress τ_0 . The effective friction force had contributions both from interface interactions and internal energy dissipation.

The following model was used to analyze the friction experiments.

$$F_{fr}^* = \mu F_l^* + \tau_0 A_{real} \quad (4)$$

$$A_{real} = \pi \left[\frac{9\pi R^2 \Delta\gamma}{4E} \left(1 + \frac{F_l^*}{3\pi R\Delta\gamma} + \sqrt{1 + \frac{2F_l^*}{3\pi R\Delta\gamma}} \right) \right]^{2/3} \quad (5)$$

where A_{real} is the real contact area, estimated according to the JKR theory, R is the radius of contacting sphere, and E and $\Delta\gamma$ are the elastic modulus and the WoA of the MAE samples, respectively.^[10] Equation (4) is often referred to as extended Amontons' law.^[10] The term, linearly dependent on the loading force F_l^* in Equation (4), corresponds to the classical Coulomb–Amontons friction between rough surfaces. The other term in the expression (4) for the friction force has a weaker dependence on the loading force (cf. Equation (5)) and corresponds to the contribution of adhesive contact. Parameters E and $\Delta\gamma$ in Equation (4) were obtained from the micro-indentation experiments. The frictional stress τ_0 and the friction coefficient μ were obtained from fitting of (3–5) to experimental data measured at different locations, using an original MATLAB program.

Statistical Analysis: For statistical analysis, ANOVA on ranks (Kruskal–Wallis test) was performed using SigmaPlot for Windows version 12.5 (Systat Software, Inc., San Jose, CA, USA). Wilcoxon rank sum test with Bonferroni correction was performed for post hoc analysis using MATLAB software (Mathworks, Natick, MA, USA). If it obeyed the logic, the groups, which distributions did not statistically differ from each other, were joined together.

Supporting Information

Supporting Information is available from the Wiley Online Library or from the author.

Acknowledgements

This work was partially supported by the German Research Foundation (DFG Grant GO 995/34-1 to SG) within Special Priority Program “Soft Material Robotic Systems.” The work of M.S. was funded by the DFG—project no. 437391117. I.B. is grateful to The State Conference of Women and Equality Officers at Bavarian Universities (LaKoF Bayern) for a Ph.D. scholarship. The authors thank Raphael Kriegl for characterization of permanent magnets.

Open Access funding enabled and organized by Projekt DEAL.

Conflict of Interest

The authors declare no conflict of interest.

Data Availability Statement

The data that support the findings of this study are openly available in Mendeley at <https://data.mendeley.com/datasets/47ggd9t42b/1>.

Keywords

friction coefficient, magnetoactive elastomer, soft robotics, surface, switchable adhesion

Received: March 16, 2022

Revised: March 24, 2022

Published online: April 20, 2022

- [1] P. Testa, B. Chappuis, S. Kistler, R. W. Style, L. J. Heyderman, E. R. Dufresne, *Soft Matter* **2020**, *16*, 5806.
- [2] M. T. Northen, C. Greiner, E. Arzt, K. L. Turner, *Adv. Mater.* **2008**, *20*, 3905.
- [3] A. G. Gillies, J. Kwak, R. S. Fearing, *Adv. Funct. Mater.* **2013**, *23*, 3256.

- [4] D.-M. Drotlef, P. Blümler, A. del Campo, *Adv. Mater.* **2014**, *26*, 775.
- [5] R. H. Ewoldt, P. Tourkine, G. H. McKinley, A. E. Hosoi, *Phys. Fluids* **2011**, *23*, 073104.
- [6] M. Watanabe, N. Wiltsie, A. E. Hosoi, K. Iagnemma, in *IEEE RSJ Int. Conf. Intell. Robots Syst.*, IEEE, Piscataway NJ, **2013**, pp. 2315–2320.
- [7] J. Krahn, E. Bovero, C. Menon, *ACS Appl. Mater. Interfaces* **2015**, *7*, 2214.
- [8] J. Risan, A. B. Croll, F. Azarmi, *J. Polym. Sci. Part B Polym. Phys.* **2015**, *53*, 48.
- [9] K. A. Daltorio, A. D. Horchler, S. Gorb, R. E. Ritzmann, R. D. Quinn, in *IEEE RSJ Int. Conf. Intell. Robots Syst.*, Piscataway NJ **2005**, pp. 3648–3653.
- [10] J. C. Mergel, R. Sahli, J. Scheibert, R. A. Sauer, *J. Adhes.* **2019**, *95*, 1101.
- [11] A. Tiwari, N. Miyashita, N. Espallargas, B. N. J. Persson, *J. Chem. Phys.* **2018**, *148*, 224701.
- [12] M. Varenberg, S. Gorb, *J. R. Soc. Interface* **2007**, *4*, 721.
- [13] K. Dening, L. Heepe, L. Afferrante, G. Carbone, S. N. Gorb, *Appl. Phys. A* **2014**, *116*, 567.
- [14] S. Song, M. Sitti, *Adv. Mater.* **2014**, *26*, 4901.
- [15] S. Reddy, E. Arzt, A. del Campo, *Adv. Mater.* **2007**, *19*, 3833.
- [16] J. Cui, D.-M. Drotlef, I. Larraza, J. P. Fernández-Blázquez, L. F. Boesel, C. Ohm, M. Mezger, R. Zentel, A. del Campo, *Adv. Mater.* **2012**, *24*, 4601.
- [17] H. Shahsavan, S. M. Salili, A. Jákli, B. Zhao, *Adv. Mater.* **2015**, *27*, 6828.
- [18] E. Kizilkán, J. Strueben, X. Jin, C. F. Schaber, R. Adelung, A. Staubitz, S. N. Gorb, *R. Soc. Open Sci.* **2016**, *3*, 150700.
- [19] E. Kizilkán, J. Strueben, A. Staubitz, S. N. Gorb, *Sci. Robot.* **2017**, *2*.
- [20] M. S. Saveleva, K. Eftekhari, A. Abalymov, T. E. L. Douglas, D. Volodkin, B. V. Parakhonskiy, A. G. Skirtach, *Front. Chem.* **2019**, *7*.
- [21] G. Filipcsei, I. Csetneki, A. Szilágyi, M. Zrínyi, in *Oligomers - Polym. Compos. - Mol. Imprinting* (Eds.: B. Gong, A.R. Sanford, J.S. Ferguson), Springer, Berlin, Heidelberg, **2007**, pp. 137–189.
- [22] Y. Li, J. Li, W. Li, H. Du, *Smart Mater. Struct.* **2014**, *23*, 123001.
- [23] A. M. Menzel, *Phys. Rep.* **2015**, *554*, 1.
- [24] Ubaidillah, J. Sutrisno, A. Purwanto, S. A. Mazlan, *Adv. Eng. Mater.* **2015**, *17*, 563.
- [25] S. Odenbach, *Arch. Appl. Mech.* **2016**, *86*, 269.
- [26] M. López-López, J. Durán, L. Iskakova, A. Zubarev, *J. Nanofluids* **2016**, *5*, 479.
- [27] M. A. Cantera, M. Behrooz, R. F. Gibson, F. Gordaninejad, *Smart Mater. Struct.* **2017**, *26*, 023001.
- [28] R. Weeber, M. Hermes, A. M. Schmidt, C. Holm, *J. Phys. Condens. Matter* **2018**, *30*, 063002.
- [29] M. Shamonin, E. Yu Kramarenko, in *Nov. Magn. Nanostructures* (Eds.: N. Domracheva, M. Caporali, E. Rentschler), Elsevier, **2018**, pp. 221–245.
- [30] T. Ohzono, M. O. Saed, Y. Yue, Y. Norikane, E. M. Terentjev, *Adv. Mater. Interfaces* **2020**, *7*, 1901996.
- [31] S. Lee, C. Yim, W. Kim, S. Jeon, *ACS Appl. Mater. Interfaces* **2015**, *7*, 19853.
- [32] C. Yang, L. Wu, G. Li, *ACS Appl. Mater. Interfaces* **2018**, *10*, 20150.
- [33] V. V. Sorokin, B. O. Sokolov, G. V. Stepanov, E. Yu. Kramarenko, *J. Magn. Magn. Mater.* **2018**, *459*, 268.
- [34] G. Glavan, P. Salamon, I. A. Belyaeva, M. Shamonin, I. Drevenšek-Olenik, *J. Appl. Polym. Sci.* **2018**, *135*, 46221.
- [35] M. Watanabe, Y. Tanaka, D. Murakami, M. Tanaka, M. Kawai, T. Mitsumata, *Chem. Lett.* **2020**, *49*, 280.
- [36] S. Chen, M. Zhu, Y. Zhang, S. Dong, X. Wang, *Langmuir* **2021**, *37*, 2312.
- [37] G. Glavan, W. Kettl, A. Brunhuber, M. Shamonin, I. Drevenšek-Olenik, *Polymers* **2019**, *11*, 594.
- [38] P. A. Sánchez, E. S. Minina, S. S. Kantorovich, E. Yu. Kramarenko, *Soft Matter* **2019**, *15*, 175.
- [39] T. A. Nadzharyan, O. V. Stolbov, Y. L. Raikher, E. Yu. Kramarenko, *Soft Matter* **2019**, *15*, 9507.
- [40] R. Li, X. Li, P. Yang, J. Liu, S. Chen, *Smart Mater. Struct.* **2019**, *28*, 085018.
- [41] S. Chen, S. Dong, X. Wang, W. Li, *Smart Mater. Struct.* **2019**, *28*, 045016.
- [42] Y. Zhou, S. Huang, X. Tian, *Adv. Funct. Mater.* **2020**, *30*, 1906507.
- [43] G. Kravanja, I. A. Belyaeva, L. Hribar, I. Drevenšek-Olenik, M. Jezeršek, M. Shamonin, *Adv. Mater. Interfaces* **2021**, *8*, 2100235.
- [44] M. Maman, V. Ponsinet, *Langmuir* **1999**, *15*, 259.
- [45] H. Pang, L. Pei, J. Xu, S. Cao, Y. Wang, X. Gong, *Compos. Sci. Technol.* **2020**, *192*, 108115.
- [46] R. Li, D. Wang, P. Yang, X. Tang, J. Liu, X. Li, *Ind. Eng. Chem. Res.* **2020**, *59*, 9143.
- [47] R. Li, Q. Xiao, P. Yang, H. Wang, L. Liu, *Mater. Des.* **2020**, *194*, 108905.
- [48] J.-H. Kim, B.-C. Kim, D.-W. Lim, B.-C. Shin, *J. Mech. Sci. Technol.* **2019**, *33*, 5321.
- [49] I. D. Johnston, D. K. McCluskey, C. K. L. Tan, M. C. Tracey, *J. Micromechanics Microengineering* **2014**, *24*, 035017.
- [50] S. Chougale, D. Romeis, M. Saphiannikova, *J. Magn. Magn. Mater.* **2021**, *523*, 167597.
- [51] A. Tiwari, L. Dorigin, A. I. Bennett, K. D. Schulze, W. G. Sawyer, M. Tahir, G. Heinrich, B. N. J. Persson, *Soft Matter* **2017**, *13*, 3602.
- [52] R. Spolenak, S. Gorb, E. Arzt, *Acta Biomater.* **2005**, *1*, 5.
- [53] M. Ruths, A. D. Berman, J. N. Israelachvili, in *Springer Handb. Nanotechnol.* (Ed.: B. Bhushan), Springer, Berlin, Heidelberg, **2004**, pp. 543–603.
- [54] *TYDEX Synthetic Sapphire*, http://www.tydexoptics.com/materials/for_transmission_optics/synthetic_sapphire/, (accessed: March 2022).
- [55] M. J. Baum, A. E. Kovalev, J. Michels, S. N. Gorb, *Tribol. Lett.* **2014**, *54*, 139.
- [56] K. L. Johnson, K. Kendall, A. D. Roberts, D. Tabor, *Proc. R. Soc. Lond. Math. Phys. Sci.* **1971**, *324*, 301.
- [57] E. Barthel, *J. Phys. D: Appl. Phys.* **2008**, *41*, 163001.
- [58] K. N. G. Fuller, D. Tabor, *Proc. R. Soc. Lond. Math. Phys. Sci.* **1975**, *345*, 327.
- [59] E. Arzt, S. Gorb, R. Spolenak, *Proc. Natl. Acad. Sci. U. S. A.* **2003**, *100*, 10603.
- [60] V. V. Sorokin, I. A. Belyaeva, M. Shamonin, E. Yu. Kramarenko, *Phys. Rev. E* **2017**, *95*, 062501.
- [61] D. V. Saveliev, I. A. Belyaeva, D. V. Chashin, L. Y. Fetisov, D. Romeis, W. Kettl, E. Y. Kramarenko, M. Saphiannikova, G. V. Stepanov, M. Shamonin, *Materials* **2020**, *13*, 3297.
- [62] P. Mazurek, S. Vudayagiri, A. L. Skov, *Chem. Soc. Rev.* **2019**, *48*, 1448.
- [63] G. Salerno, M. Rebora, A. Kovalev, E. Gorb, S. Gorb, *J. Comp. Physiol. A* **2018**, *204*, 627.
- [64] S. Gorb, Y. Jiao, M. Scherge, *J. Comp. Physiol. A* **2000**, *186*, 821.
- [65] D. M. Ebenstein, K. J. Wahl, *J. Colloid Interface Sci.* **2006**, *298*, 652.